Energy Management System for an Islanded Microgrid With Convex Relaxation

Muhammad Fahad Zia, *Student Member, IEEE*, Elhoussin Elbouchikhi, *Senior Member, IEEE*, Mohamed Benbouzid, *Senior Member, IEEE*, and Josep M. Guerrero, *Fellow, IEEE*

***Abstract*—Conventional energy generation sources mainly provide energy supply to remote areas nowadays. However, because of growing concerns over greenhouse gas emissions, the integration of renewable energy sources is mandatory to meet power demands and reduce climatic effects. The advancements in renewable generation sources and battery storage systems pave the way for microgrids (MGs). As a result, MGs are becoming a viable solution for power supply shortage problems in remote-area applications, such as oceanic islands. In this paper, an islanded MG, which consists of PV system, tidal turbine (TT), diesel generator (DG), and Li-ion battery, is considered for Ouessant island in Brittany region in France. The economic operation of the MG is achieved by including battery degradation cost, levelized costs of energy of the PV system and TT, operating and emission costs of DG, and network constraints. The developed model leads to a non-linear and non-convex problem, which unfortunately can converge to a local optimum solution. The problem has, therefore, been relaxed and converted to a convex second-order cone model to achieve an optimal decision strategy for islanded MG operations with a global or near-global solution. Numerical simulations are carried out to prove the effectiveness of the proposed strategy in reducing the operating and emission costs of the islanded MG. It is shown that the developed convex energy management system formulation has an optimality gap of less than 1% with reduced computational cost.**

***Index Terms*—Convex optimization, demand response (DR), energy management system (EMS), island, microgrid (MG), PV system, second-order cone programming, tidal turbine (TT).**

I. Introduction

RENEWABLE energy sources (RESs) have gained the attention of industrialists, scientists, and environmentalists because of the exponential rise in global energy demand and drastic climatic effects with increased greenhouse gas (GHG) emissions. The advancement and maturity in RES technologies have paved the way for their large-scale deployment to meet the goals of the Paris climate agreement. However, RESs have volatility and intermittent problems, which can be resolved by integrating them with energy storage systems and small-scale conventional generation sources. This integration arises energy scheduling and control problems of these distributed energy sources. The microgrid (MG), a low-voltage network, provides the solution to these problems with an ability to operate both in grid-connected and standalone modes [1]–[3].

Numerous islands and other remote areas have no access to utility grid because of high investment cost in transmission systems. Therefore, local demand is partially supplied by conventional generation sources, mainly diesel generators (DGs) [4]. However, the continuous availability of diesel fuel and high GHG emissions of these DGs are big problems for these remote areas. Fortunately, RESs, such as solar-, wind-, and tidal-energy (TE) sources, can be used to meet local energy demand and solve these problems.

Marine RESs can play a vital role in meeting the electricity demand of island occupants. Marine RESs consist of ocean thermal energy, ocean osmosis energy, TE, and wave energy sources. The global ocean energy potential is expected to be more than 300 GW in installed capacity by the year 2050 [5]. TE has currently huge potential among these marine RESs because of relatively mature turbine technologies and higher accuracy in tidal speed prediction.

The gravitational motion of the moon and sun causes periodic oscillation of the sea level, called tide in the literature. It has the same convectional properties of wave, such as amplitude and wavelength. The TE potential is around 75 GW worldwide and 11 GW in Europe. In Europe, the U.K. and France are leading with TE potential of 6 and 3.4 GW, respectively [6]. Worlds' first tidal power station of 240 MW is also located on the La Rance river in Brittany. Tidal industry is expanding with more than 100 companies working on it worldwide. The EU accounts for more than 50% of the tidal developers [7].

TE can be harnessed by using mainly two methods: 1) tidal barrage; and 2) tidal turbines (TTs). In the tidal-barrage method, generator produces electric energy from turbine movements with water flow, which is controlled by opening and closing barrage's sluices with the rise and fall of the tidal level. It is being used in tidal power stations at Sihwa Lake in South-Korea and La Rance in France. However, tidal barrages lack promising developments in the future because of limited potential sites, immense

Manuscript received March 1, 2019; revised May 8, 2019; accepted May 9, 2019. Date of publication May 15, 2019; date of current version November 7, 2019. Paper 2018-BAMM-1335.R1, approved for publication in the IEEE TRANSACTIONS ON INDUSTRY APPLICATIONS by the Building Automation, Metering and Microgrids for Energy Efficiency in Industrial and Commercial Power Systems of the IEEE Industry Applications Society. *(Corresponding author: Mohamed Benbouzid.)*

M. F. Zia is with the University of Brest, UMR CNRS 6027 IRDL, Brest 29238, France (e-mail: muhammadfahad.zia@univ-brest.fr).

E. Elbouchikhi is with ISEN Yncréa Ouest, UMR CNRS 6027 IRDL, 29200, Brest, France (e-mail: elhoussin.elbouchikhi@isen-ouest.yncrea.fr).

M. Benbouzid is with the University of Brest, UMR CNRS 6027 IRDL, Brest 29238, France, and also with Shanghai Maritime University, Shanghai 201306, China (e-mail: mohamed.benbouzid@univ-brest.fr).

J. M. Guerrero is with the Department of Energy Technology, Aalborg University, Aalborg 9220, Denmark (e-mail: joz@et.aau.dk).

Color versions of one or more of the figures in this paper are available online at http://ieeexplore.ieee.org.

Digital Object Identifier 10.1109/TIA.2019.2917357

capital investment, and negative effects on marine environment [8]. Contrarily, TTs have gained huge attention worldwide, as they require less capital investment for large-scale energy extraction. TTs lead in technology maturity among other marine energy technologies, which is obvious from their technology readiness level [9].

In Europe, Brittany region in France is among the regions with huge TE potential. The local energy demand of the islands in Brittany region, such as Ouessant island, can be met by using TTs along with other energy sources. Hence, MG system sizing was performed in [10], where the authors have achieved the optimal sizing of a hybrid power generation system. It comprises PV system, TT, wind turbine, and battery storage system. In [11], wind, tidal, and pumped hydro storage-based MG system was proposed and designed to reduce GHG emissions. However, the industrial proposal for Ouessant island include DG, PV system, TT, and Li-ion battery system. Therefore, an islanded MG, which consists of PV system, TT, DG, and Li-ion battery, has been designed to meet the electricity demand of the island. In this regard, we proposed an islanded marine MG system for Ouessant island in [12]. An energy management system (EMS) was developed to minimize the MG system operating cost. However, the developed EMS is non-convex. Moreover, it does not include DG GHG emissions and demand response (DR) in MG operation.

Islanded MGs require EMS to optimize their daily energy scheduling operation [13]. An EMS receives energy-generation and load-demand information from all local sources, and it determines the decision strategies for each local source by performing optimization on various objectives [1]. Various EMS approaches have already been proposed in the literature. In [14], optimal EMS was developed for PV and fuel cell based MG to minimize its operating cost. A linear-programming (LP) EMS was developed for grid-connected MG with tidal generation and pumped hydro storage system in [15]. Sukumar *et al.*[16] developed EMS models based on LP and on mixed integer linear programming (MILP). MILP-based MG EMSs were developed and experimentally validated in [17] and [18]. Conte *et al.* [19] developed an MILP model for the optimal dispatch of PV and storage-based MGs. Another MILP model was presented in [20] for residential MG EMSs by applying Taylor-series approximation, estimation operation points, and auxiliary variables based methods on the original non-linear problem. The developed model achieved solution error below 2% with fewer computations. Solanki *et al.* [21] proposed the operating- and emission-cost based mixed integer quadratic EMS model for isolated MGs, and they also studied DR impacts on MG operation. Solanki *et al.* [22] presented a mixed integer non-linear programming (NLP) model to incorporate DR into MG EMSs. It achieved the objective of minimizing the operating cost of the DGs and penalty cost on energy curtailment with higher number of computations. A mixed integer second-order cone programming based EMS model was developed in [23], which minimizes the load shedding cost of isolated MGs. However, integer variables increase computations and cause convergence problems. Moreover, they lack in providing solutions against TT-based islanded MG EMSs, battery degradation cost consideration, and DR computations at each bus.

In this context, this paper aims at developing integer-free second-order cone programming based EMS (SOCP-EMS) model to minimize the operating and emission costs of islanded MGs. The proposed model includes the operating and emission costs of DG, levelized costs of energy (LCOEs) of TT and PV system, battery degradation cost, generation sources and battery operational constraints, incentive-based DR model, and ac power flow, and it guarantees global optimality. To the best knowledge of the authors, no SOCP-EMS model with these characteristics has been proposed for MGs [1], [24].

The main contributions of this paper are as follows.

1) Optimal EMS model is proposed to enable effective integration of the RESs, DG, and local energy storage into islanded MGs.
2) TT integration and modeling in islanded MG EMSs is included.
3) An incentive-based DR scheme is introduced for the active participation of consumers.
4) Convex-SOCP model is proposed for the developed non-convex EMS problem.
5) Integer-free EMS model substantially reduces the number of computations, thus paving the way for real-time implementation in MGs.

The rest of this paper is organized as follows. Section II presents islanded MG's architecture and models its components. Section III develops a non-linear EMS optimization problem. Section IV converts the proposed non-convex EMS problem into relaxed convex SOCP model. Section V presents the simulation setup and results. Finally, conclusion is presented in Section VI.

II. Islanded MG Model

Ouessant island, (48°28′N, 5°5′W), is considered as a case study for islanded marine MGs. It is located in Brittany region in France with a total population of 862 inhabitants. It has huge TE potential in Fromveur strait [25], [26], and electric power can be produced up to 500 MW [27].

A. System Architecture

The marine MG system is the most suitable power system for islands with marine energy potential. Therefore, an islanded marine MG system is proposed in Fig. 1. It consists of PV system, TT, DG, Li-ion battery, and power converters. It also includes an island power network to consider system losses and buses voltages. The power demand is divided into two categories, namely critical and responsive loads (RLs). The RLs are used for DR operation in MG energy scheduling. MGs require local controllers (LCs) and MG central controller (MGCC) to share information and data using efficient communication technologies. The communication technologies are mainly selected on the basis of coverage area, data rate, and deployment cost [1]. Wireless communication technologies are better options for marine MG systems at islands. LCs and MGCC share information to optimize the operation of MG EMSs.

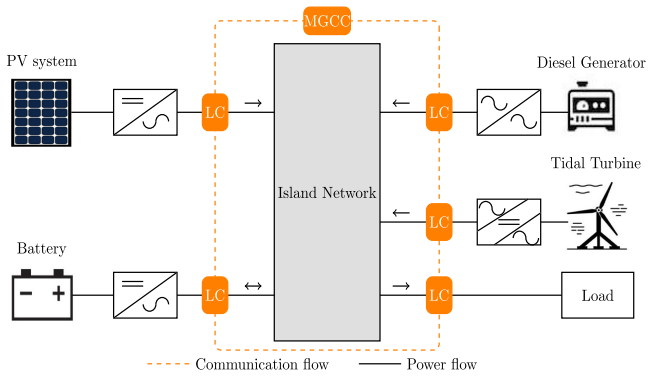

Fig. 1. Islanded ac MG architecture.

B. Diesel Generator

DGs are the only major energy sources in islands. They often partially meet the energy demand. They operate with RESs to provide continuous power supply to load ends. DGs have higher operating costs in islands because of high transportation cost. The following is the operating cost model of DG [11]:

$$OC_t^g = a(P_t^g)^2 + aP_t^g + c, \quad t \in \mathcal{T} \tag{1}$$

where a, b, and, c are DG cost coefficients. P_t^g is DG scheduled output power at time t.

DGs have higher amount of GHG emissions, which adversely affect the global climate. Therefore, the emission cost of DG is modeled as

$$EC_t^g = \pi^e E^g P_t^g, \quad t \in \mathcal{T}. \tag{2}$$

DG emission cost includes the equivalent lifecycle carbon emissions, E^g, and penalty cost on them, π^e, to achieve the objective of environmental sustainability.

C. Tidal Turbine

TTs convert the kinetic energy of tidal streams into electric energy. TTs are installed underwater, thus creating an obstruction at sea surface level. TTs are mainly categorized as horizontal-axis TTs, vertical-axis TTs, duct-type TTs, oscillating-hydrofoil TTs, and tidal-kite TTs [28], [29]. In [30], a critical analysis on different TTs' drivetrain options was presented to compare their performances, which helps in selecting TTs for marine energy conversion systems.

Tidal speed can be calculated from (3) by using spring tidal speed, $\upsilon_{sm,t}$, and neap tidal speed, $\upsilon_{nm,t}$, information at the reference location. We have

$$\upsilon_{m,t} = \upsilon_{nm,t} + \frac{(C - \gamma_{nm})(\upsilon_{sm,t} - \upsilon_{nm,t})}{\gamma_{sm} - \gamma_{nm}} \tag{3}$$

where C is the tidal coefficient, which estimates the amplitude of tides forecasts. γ_{sm} and γ_{nm} are the tidal coefficients of the spring and neap tides, respectively.

A TT's output power depends on turbine swept area, turbine power coefficient, and tidal speed. The estimated output power, $P_{a,t}^m$, is determined using (4). A TT cannot produce power below cut-in tidal speed, υ_{ci}. The output power increases with tidal speed until it reaches its maximum power at rated tidal speed, υ_r. It produces the maximum power above the rated tidal speed. However, it stops producing electric power after cut-out tidal speed, υ_{co}, to avoid the structural damage in TTs.

$$P_{a,t}^m = \begin{cases} 0, & \upsilon_t < \upsilon_{\text{ci}} \\ \frac{1}{2}\rho\wp^m \pi R^2 \upsilon_t^3, & \upsilon_{\text{ci}} \le \upsilon_t < \upsilon_r \\ \frac{1}{2}\rho\wp^m \pi R^2 \upsilon_r^3, & \upsilon_r \le \upsilon_t \le \upsilon_{\text{co}} \\ 0, & \upsilon_t > \upsilon_{\text{co}} \end{cases} \quad t \in \mathcal{T} \tag{4}$$

where ρ is the water density. $\wp^m$ and πR^2 are TT power coefficient and swept area, respectively. The TT's operational cost is modeled as

$$OC_t^m = C^m P_t^m, \quad t \in \mathcal{T}. \tag{5}$$

The LCOE criteria is used to determine TT's electricity production cost, C^m, in (6). It comprises investment cost, C_{inv}^m (€), operation and maintenance costs, C_{om}^m (€ /year), annual energy output, E_{an}^m, discount rate dr, and TT degradation factor, σ^m. We have

$$C^m = \frac{C_{\text{inv}}^m + \sum_{i=1}^n C_{\text{om}}^m (1+dr)^{-i}}{\sum_{i=1}^n E_{\text{an}}^m (1-\sigma^m)^{i-1}(1+dr)^{-i}}. \tag{6}$$

The discount rate, dr, is used to compute the yearly present values of C_{om}^m and E_{an}^m over system lifetime of n years. σ^m accounts for the degradation in TT's annual energy output after the first year. σ^m accounts for bio-fouling, salts-induced material corrosion, marine creatures, flotsam, and blade cavitation effects in the degradation of TTs [31].

D. PV System

A PV system's available output power, $P_{a,t}^s$, is calculated using (7) [32]. It computes the available output power of the PV system by using solar irradiance, G_t, and temperature, T_t, data at each time t. We have

$$P_{a,t}^s = N^s P_{\text{STC}}^s \left[\frac{G_t}{G_{\text{STC}}} (1 - \gamma(T_{c,t} - T_{\text{STC}})) \right], \; t \in \mathcal{T} \tag{7}$$

where N^s is the number of PV arrays. G_{STC}, T_{STC}, and P_{STC}^s, are irradiance, temperature, and PV array output power at standard test conditions, respectively. γ is the temperature-dependent degradation coefficient. $T_{c,t}$ is PV cell's temperature, and it is computed as

$$T_{c,t} = T_t + \frac{G_t}{G_{\text{NOCT}}} (\text{NOCT} - 20), \quad t \in \mathcal{T} \tag{8}$$

where G_{NOCT} is the irradiance at nominal operating cell temperature.

The PV system's operational cost, OC_t^s, is provided by

$$OC_t^s = C^s P_t^s, \quad t \in \mathcal{T} \tag{9}$$

where C^s is the LCOE of the PV system in the units of € /kWh, and it is modeled as

$$C^s = \frac{C_{\text{inv}}^s + \sum_{i=1}^n C_{\text{om}}^s (1+dr)^{-i}}{\sum_{i=1}^n E_{\text{an}}^s (1-\sigma^s)^{i-1}(1+dr)^{-i}}. \tag{10}$$

The LCOE model of the PV system includes investment cost, C^s_{inv}, operation and maintenance costs, C^s_{om}, annual energy output, E^m_s, discount rate dr, and PV system's degradation factor, σ^s. The discount rate is used to compute the yearly present values of C^s_{om} and E^s_{an} over system lifetime of n years. σ^s accounts for the degradation in the PV system's annual energy output after the first year.

E. Battery

Li-ion batteries have gained huge attention among other batteries because of their high energy density and technology maturity. Let OC^b_t and C^b_t denote the battery's operational and degradation costs at time t, respectively. The battery's operational cost each with charging efficiency, η^{b+}, and discharging efficiency, η^{b-}, is modeled as

$$OC^b_t = C^b_t \left(\eta^{b+} P^{b+}_t + \frac{P^{b-}_t}{\eta^{b-}} \right), \quad t \in \mathcal{T} \tag{11}$$

where P^{b+}_t and P^{b-}_t are battery's charging and discharging powers at time t, respectively.

The degradation cost model includes the depth of discharge (DOD) and temperature-dependent capacity- and power-fading effects of battery. The degradation cost is calculated as [32]

$$C^b = \frac{1}{2} \frac{\left[C^b_{\text{inv}} + \sum_{i=1}^{n} C^b_{\text{om}} (1+dr)^{-i}\right](1+dr)^n - SV}{(1+dr)^n \chi^E_T \chi^{\Upsilon}_T \chi^{\Upsilon}_d \Upsilon^b_r E^b_r} \tag{12}$$

where χ^E_T is the normalized temperature-dependent power-fading coefficient. χ^{Υ}_T and χ^{Υ}_d are the temperature- and DOD-dependent capacity-fading coefficients. The regression modeling of these coefficients is detailed in [32]. Υ^b_r and E^b_r are the rated cyclelife and energy capacity of battery. Salvage value (SV) is the value of battery at the end of its useful life.

The charge (discharge) rates control the charging (discharging) power of battery, which are defined as

$$P^{b+}_t = l^+_t E^b_r, \quad t \in \mathcal{T} \tag{13}$$

$$P^{b-}_t = l^-_t E^b_r, \quad t \in \mathcal{T} \tag{14}$$

where l^+_t and l^-_t are battery's charge and discharge rates, respectively.

The degradation-cost variation for each month is shown as the boxplot in Fig. 2 for Ouessant island. It is low in the months of July and August, while higher in December, January, and February for a fixed DOD ($d = 0.5$). Hence, the battery's operational cost will be higher in winter because of low temperature.

F. Demand Response

MG operators offer incentives to consumers against the control of RL shifting. The operator receives the RL's data, which includes their proportion of total load and set of shifting instants, $\mathcal{T}_s$. The shifting instants can be forward, backward, or both. RLs, $D^r = D^{pr} + jD^{qr}$, are deferred to the scheduled ones, and consumers will get the incentives in return. D^{pr} and D^{qr} are RL's active and reactive components, respectively. Equation (15) defines the shifting of RL's active power from instant t to i, while

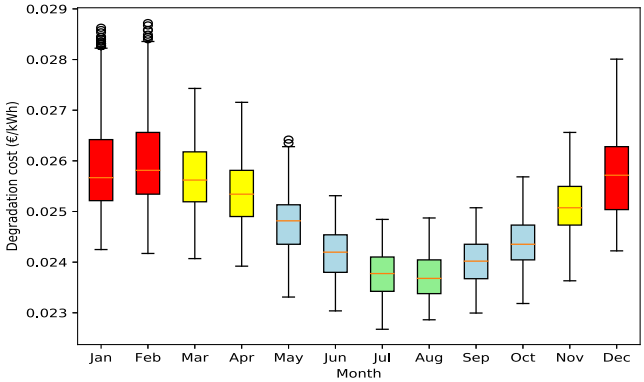

Fig. 2. Battery degradation cost variation at 50% DOD.

their recovering is modeled in (16).

$$D^{pr+}_{x,t} = \sum_{\substack{i \in \mathcal{T}_s \\ i \neq t}} D^{pr}_{x,t,i}, \quad x \in \mathcal{N}_{\mathcal{X}}, t \in \mathcal{T} \tag{15}$$

$$D^{pr-}_{x,t} = \sum_{\substack{i \in \mathcal{T}_s \\ i \neq t}} D^{pr}_{x,i,t}, \quad x \in \mathcal{N}_{\mathcal{X}}, t \in \mathcal{T} \tag{16}$$

where $D^{pr+}_{x,t}$ and $D^{pr-}_{x,t}$ are RL shifted and recovered active powers at load Bus x and time t, respectively. RL active and reactive powers are strongly correlated: If RL active power is increased or decreased, its reactive power will do the same. Therefore, it is assumed that RL active and reactive powers can be related with one reasonable method: RL power factor remains constant, which means that $D^{qr}_{x,t} = D^{pr}_{x,t} \tan \phi_x$, and ϕ_x is the RL power-factor angle at Bus x.

The incentive cost for MG operator is

$$IC^r_t = \sum_{x \in \mathcal{N}_{\mathcal{X}}} \beta^r D^{pr+}_{x,t}, \quad t \in \mathcal{T} \tag{17}$$

where β^r corresponds to the fixed incentive rate for consumers against RL shifting.

G. Network Model

Consider an islanded MG consisting of $\mathcal{N}$ buses. Active power, $P_{i,t}$ and reactive power, $Q_{i,t}$, are the difference of generation and load, critical and RLs, at each Bus i and time t. The network model is incorporated into MG EMS to achieve its operation within the operating voltage limits and system losses restriction. The power flow equations of the network model are

$$P_{i,t} = \sum_{\substack{j=1 \\ j \neq i}}^{\mathcal{N}} \Re \left\{ \underline{V}_{i,t} (\underline{V}^*_{i,t} - \underline{V}^*_{j,t}) y^*_{ij} \right\}, \; i,j \in \mathcal{N}, t \in \mathcal{T} \tag{18}$$

$$Q_{i,t} = \sum_{\substack{j=1 \\ j \neq i}}^{\mathcal{N}} \Im \left\{ \underline{V}_{i,t} (\underline{V}^*_{i,t} - \underline{V}^*_{j,t}) y^*_{ij} \right\} \; i,j \in \mathcal{N}, t \in \mathcal{T} \tag{19}$$

where $\underline{V}_{i,t}$ is the complex voltage of Bus i at time t. y_{ij} is the branch admittance between Buses i and j, and $y_{ij} = \frac{1}{r_{ij} + j x_{ij}}$.

r_{ij} and x_{ij} are the branch resistance and reactance between Buses i and j, respectively.

III. Energy Management Model

Consider an islanded MG of an $\mathcal{N}$-bus system. The EMS model is developed to optimize the MG operation over a scheduling horizon $\mathcal{T} := \{t_s, t_s + \Delta t, t_s + 2\Delta t, \ldots, t_f\}$. The model aims to minimize the islanded MG's operating and emission costs, which comprises DG operating and emission costs, LCOEs of PV system and TT, battery degradation cost, and DR incentive cost. The cost relations of RESs and battery storage systems comprises investment cost, operation and maintenance costs, and degradation parameters. The following are the details of the proposed model:

$$\min \sum_{t\in\mathcal{T}} \{OC_t^g + EC_t^g + OC_t^m + OC_t^s + OC_t^b + IC_t^r\}\,\Delta t \tag{20a}$$

s.t. (1), (2), (6), (11), (13), (15)–(44)

$$P^g_{\min} \le P^g_t \le P^g_{\max}, \quad t \in \mathcal{T} \tag{20b}$$

$$Q^g_{\min} \le Q^g_t \le Q^g_{\max}, \quad t \in \mathcal{T} \tag{20c}$$

$$0 \le P^m_t \le P^m_{a,t}, \quad t \in \mathcal{T} \tag{20d}$$

$$0 \le P^s_t \le P^s_{a,t}, \quad t \in \mathcal{T} \tag{20e}$$

$$(P^m_t)^2 + (Q^m_t)^2 \le (S^m)^2, \quad t \in \mathcal{T} \tag{20f}$$

$$(P^s_t)^2 + (Q^s_t)^2 \le (S^s)^2, \quad t \in \mathcal{T} \tag{20g}$$

$$0 \le l^+_t \le l^+_{\max}, \quad t \in \mathcal{T} \tag{20h}$$

$$0 \le l^-_t \le l^+_{\max}, \quad t \in \mathcal{T} \tag{20i}$$

$$l^+_t l^-_t = 0, \quad t \in \mathcal{T} \tag{20j}$$

$$E^b_t = E^b_{t-1} + \left[\eta^+ P^{b+}_t - \frac{P^{b-}_t}{\eta^-}\right]\Delta t,\ t \in \mathcal{T} \tag{20k}$$

$$E^b_{t_f} = E^b_{t_s} \tag{20l}$$

$$E^b_{\max} = E^b_r \chi^{\Xi}_{\mu_T} \tag{20m}$$

$$E^b_{\min} = E^b_{\max}(1-d) \tag{20n}$$

$$E^b_{\min} \le E^b_t \le E^b_{\max} \tag{20o}$$

$$(P^{b+}_t - P^{b-}_t)^2 + (Q^b_t)^2 \le (S^b)^2, \quad t \in \mathcal{T} \tag{20p}$$

$$D^{pr+}_{x,t} D^{pr-}_{x,t} = 0, \quad x \in \mathcal{N}_{\mathcal{X}}, t \in \mathcal{T} \tag{20q}$$

$$\sum_{t\in\mathcal{T}} D^{pr+}_{x,t} = \sum_{t\in\mathcal{T}} D^{pr-}_{x,t}, \quad x \in \mathcal{N}_{\mathcal{X}} \tag{20r}$$

$$D^{pr}_{x,t,i} \le D^{pr}_{x,t,\max}, \quad x \in \mathcal{N}_{\mathcal{X}}, t \in \mathcal{T} \tag{20s}$$

$$D^{pr+}_{x,t} \le D^{pr}_{x,t,\max}, \quad x \in \mathcal{N}_{\mathcal{X}}, t \in \mathcal{T} \tag{20t}$$

$$D^{pr+}_{x,t}, D^{pr-}_{x,t} \ge 0, \quad x \in \mathcal{N}_{\mathcal{X}}, t \in \mathcal{T} \tag{20u}$$

$$P^g_t + P^m_t + P^s_t - P^{b+}_t + P^{b-}_t + \sum_{x\in\mathcal{N}_{\mathcal{X}}} \left(D^{pr+}_{x,t} - D^{pr-}_{x,t}\right) \le (1+\alpha) D^p_t, t \in \mathcal{T} \tag{20v}$$

$$V_{i,\min} \le V_{i,t} \le V_{i,\max}, \quad i \in \mathcal{N}, t \in \mathcal{T} \tag{20w}$$

$$\theta_{ij,\min} \le \measuredangle \underline{V}_{i,t} - \measuredangle \underline{V}_{j,t} \le \theta_{ij,\max}, \quad i,j \in \mathcal{N}, t \in \mathcal{T} \tag{20x}$$

where $\measuredangle \underline{V}_{i,t}$ is the phase angle of complex voltage $\underline{V}_{i,t}$ at Bus i. $\theta_{ij,\min}$ and $\theta_{ij,\max}$ are the minimum and maximum limits on phase-angle difference between Buses i and j, respectively.

Constraints (20b) and (20c) define the operational limits on DG active and reactive powers output, respectively. (20d) and (20e) represent the limits on the output active power from TT and PV system, respectively. The inverters capabilities of TT and PV system are provided in convex quadratic inequalities (20f) and (20g), respectively [33]–[35]. S^m_t and S^s_t are the apparent power ratings of TT and PV inverters, respectively. Constraints (20h) and (20i) ensure that the battery's charging and discharging operations remain within the limits of maximum allowable charge (discharge) rates, respectively. Constraint (20j) prohibits battery's concurrent charging and discharging operations. The dynamic energy state representation of the battery is provided in (20k). Constraint (20l) ensures that the battery's initial and final energy states remain the same. Constraints (20m)–(20o) represent the limits on the battery's energy state. Constraint (20p) corresponds to the reactive-power capability of battery inverter [36]. Constraint (20q) prohibits the simultaneous shifting and recovering of RL. Constraint (20r) ensures that the total shifted and recovered RLs are the same. Inequalities (20s)–(20u) represent RL limits. Constraint (20v) stands for limiting the total active-power losses, with α representing the allowable active-power losses ratio. Constraints (20w) and (20x) correspond to the limits on bus voltage magnitude and buses' phase angle difference, respectively.

IV. Convex Formulation

MG EMS problem (20a) is intrinsically a non-convex NLP model because of battery constraint (20j), DR constraint (20p), and network constraints (18) and (19). It arises local optimality issues. However, these constraints can be relaxed into convex ones [37]. Battery constraints (20h)–(20j) are modified into the following mixed integer linear equations:

$$0 \le l^+_t \le \delta_t\, l^+_{\max}, \quad t \in \mathcal{T} \tag{21a}$$

$$0 \le l^-_t \le (1-\delta_t)\, l^-_{\max}, \quad t \in \mathcal{T} \tag{21b}$$

$$\delta_t \in \{0,1\}, \quad t \in \mathcal{T} \tag{21c}$$

where δ_t is a binary variable for battery at instant t. However, these binary variables may cause higher computation burden, thus making solution time more expensive. Therefore, binary constraint (21c) is relaxed into the continuous one (21d). We have

$$0 \le \delta_t \le 1, \quad t \in \mathcal{T}. \tag{21d}$$

DR constraint (20q) is also non-convex and non-linear, which is converted into convex linear constraints (22a) by also replacing equations (20t) and (20u). We have

$$0 \le D^{pr+}_{x,t} \le \xi_{x,t}\, D^{pr}_{x,t,\max}, \quad x \in \mathcal{N}_{\mathcal{X}}, t \in \mathcal{T} \tag{22a}$$

$$0 \le D^{pr-}_{x,t} \le (1-\xi_{x,t})\, M, \quad x \in \mathcal{N}_{\mathcal{X}}, t \in \mathcal{T} \tag{22b}$$

$$0 \le \xi_{x,t} \le 1, \quad x \in \mathcal{N}_{\mathcal{W}}, t \in \mathcal{T} \tag{22c}$$

where M is a large number, and islanded MG operator can chose it on the basis of peak demand limit. It should not be very large to avoid convergence problems.

MG network's power flow constraints (18) and (19) are non-convex because of voltage product component, $\underline{V}_{i,t}\underline{V}^*_{j,t}$. These equations can be convexified using existing methods in the literature [38]–[40]. In this paper, the SOCP method is preferred over semi-definite programming because of its lower computational complexity [41]. Let $\underline{H}_{ij,t} = \underline{V}_{i,t}\underline{V}^*_{j,t}$, and constraints (18), (19), (20w), (20x), are transformed into the following [42], [43]:

$$P_{i,t} = \sum_{\substack{j=1 \\ j\neq i}}^{\mathcal{N}} \Re\left\{(\underline{H}_{ii,t} - \underline{H}_{ij,t}) y^*_{ij}\right\},\ i,j \in \mathcal{N}, t \in \mathcal{T} \tag{23a}$$

$$Q_{i,t} = \sum_{\substack{j=1 \\ j\neq i}}^{\mathcal{N}} \Im\left\{(\underline{H}_{ii,t} - \underline{H}_{ij,t}) y^*_{ij}\right\},\ i,j \in \mathcal{N}, t \in \mathcal{T} \tag{23b}$$

$$V^2_{i,\min} \le H_{ii,t} \le V^2_{i,\max},\ i \in \mathcal{N}, t \in \mathcal{T} \tag{23c}$$

$$\tan(\theta_{ij,\min}) \le \frac{\Im\left\{\underline{H}_{ij,t}\right\}}{\Re\left\{\underline{H}_{ij,t}\right\}} \le \tan(\theta_{ij,\max}) \quad i,j \in \mathcal{N}, t \in \mathcal{T}\ . \tag{23d}$$

The non-convexity in $H_{ij,t} = V_{i,t}V^*_{j,t}$ is converted into convex SOC form as

$$H_{ij,t} \le H_{ii,t} H_{jj,t}, \quad i,j \in \mathcal{N}, t \in \mathcal{T}. \tag{23e}$$

MG's non-convex EMS model (20a) is transformed into relaxed convex SOCP model as

$$\begin{aligned} \min \quad & \sum_{t\in\mathcal{T}} \{OC^g_t + EC^g_t + OC^m_t + OC^s_t \\ & + OC^b_t + IC^r_t\}\, \Delta t \\ \text{s.t.} \quad & (1), (2), (6), (11), (13), (15)\text{–}(17), (21)\text{–}(28), \\ & (21)\text{–}(26), (30)\text{–}(35), (37), (38), (41), \\ & (44), (45), (47), (48), (51). \end{aligned} \tag{24}$$

This relaxed convex SOCP-EMS model can be solved by Gurobi [44], while the non-convex EMS model is solved by IPOPT [45] in GEKKO Python [46]. The relaxed SOCP model solution is feasible and globally optimum, if it satisfies the original non-convex EMS problem constraints.

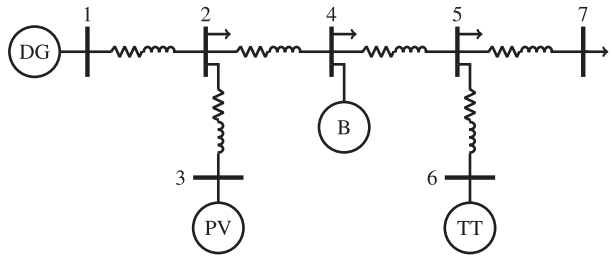

Fig. 3. 7-bus MG test network.

TABLE I
7-BUS MG TEST NETWORK DATA

Br. no.	Rx. nd.	Sn. nd.	R (Ω)	X (Ω)
1	1	2	0.482	0.062
2	2	3	0.233	0.017
3	2	4	0.416	0.035
4	4	5	0.165	0.021
5	5	6	0.642	0.083
6	5	7	0.416	0.035

TABLE II
TECHNICAL DATA

Diesel generator					
a, b, c	0.01, 0.5, 0	E^g (g/kWh)	778	π^e (€/kWh)	35
P^g_{min}, P^g_{max} (kW)	0.5, 6	Q^g_{min}, Q^g_{max} (kVAR)	-1, 4		
Tidal turbine					
C^m_{inv} (€/kW)	3500	C^m_{om} (€/kW–year)	140	C^m (€/kWh)	0.232
Rated Power (kW)	3	σ^m (%)	2	S^m (kVA)	3.2
v_{ci} (m/s)	0.5	v_r (m/s)	2.7	v_{co} (m/s)	5
γ_{sm}	95	γ_{nm}	45	R (m)	0.5
PV sytem					
C^s_{inv} (€/kW)	1930	C^s_{om} (€/kW–year)	22	C^s (€/kWh)	0.148
Rated Power (kW)	4	σ^s (%)	0.05	S^s (kVA)	4.3
Li-ion battery					
C^b_{inv} (€/kWh)	200	C^b_{om} (€/kW–year)	20	η^{b+}, η^{b-}	0.9
E^b_r (kWh)	10	d (%)	0.5	S^b (kVA)	5.3

V. SIMULATION SETUP AND RESULTS

The proposed SOCP-EMS is tested on a 7-bus islanded MG, as shown in Fig. 3. It consists of DG at root Bus 1, PV system at Bus 3, battery at Bus 4, and TT at Bus 6. Buses 2, 4, 5, and 7 are load buses. MG is a low-voltage network; therefore, system voltage is assumed to be 230 V. The network data of the islanded MG are provided in Table I. The line impedances are set following the criteria of $\frac{R}{X}$ ratio to be at least 7.7 in distribution system [47], [48]. The scheduling horizon is considered 24 h. Table II presents the technical data of DG, TT, PV, and battery. The maximum charge and discharge rates of the battery are bounded by 0.5 each. The SV of the battery is assumed to be 40% of the capital cost. The discount rate is considered 4%. Four cases are considered to study the effectiveness of the proposed EMS model for a 24-h period. The battery remains operational in all the following cases:

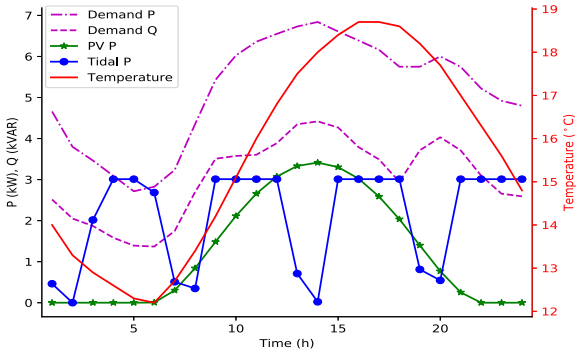

Fig. 4. PV, TT, load, and temperature data for July.

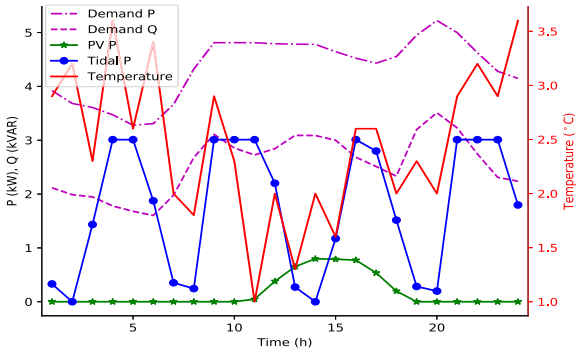

Fig. 5. PV, TT, load, and temperature data for December.

1) Case I: All DG, PV, and TT units are online for July.
2) Case II: Only PV system is off-line for July.
3) Case III: Only TT is off-line for July.
4) Case IV: All DG, PV, and TT units remain online for December.

Figs. 4 and 5 present the temperature, PV power, TT power, and demand profiles of Ouessant island for the 24-h period in July and December, respectively. The active and reactive demands at load Buses 2, 4, 5, and 7 are assumed to be 35%, 15%, 25%, and 25% of the total demand, respectively. The DR power factor for each load bus is considered to be 0.85 for this case study. The fixed DR incentive is assumed to be 15 € /MWh. The RL is considered 20% of the base active load. The maximum limit on the active power losses is considered 5% of the total active demand for the islanded MG network. The bus voltage deviations are limited within ± 5%. All the simulations are performed on an i5 2.8-GHz processor with 16 GB RAM.

A. *SOCP-EMS Performance*

The proposed SOCP-EMS is evaluated by measuring the optimality gap between the original non-convex EMS and relaxed SOCP-EMS using the following formula:

$$\text{optimality gap} = \frac{\text{original EMS} - \text{relaxed EMS}}{\text{original EMS}}. \quad (25)$$

The optimality gap is less than 1% for each case, as shown in Table III. Moreover, the SOCP–EMS runtime is far better than that of a non-convex EMS in each case. It proves that the proposed

TABLE III
SOCP-EMS PERFORMANCE

	Non-convex EMS		SOCP-EMS		
	Obj. value (€)	Runtime (s)	Obj. value (€)	Optimality gap (%)	Runtime (s)
Case-I	41.304	213.2	41.025	0.68	6.23
Case-II	53.901	156.7	53.891	0.02	6.84
Case-III	57.695	124.3	57.254	0.08	7.21
Case-IV	44.713	169.3	44.578	0.30	5.86

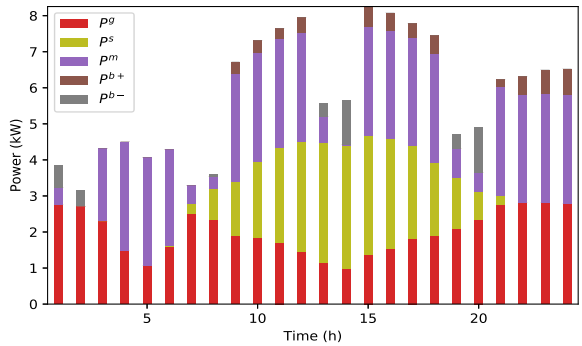

Fig. 6. Islanded MG scheduling profile.

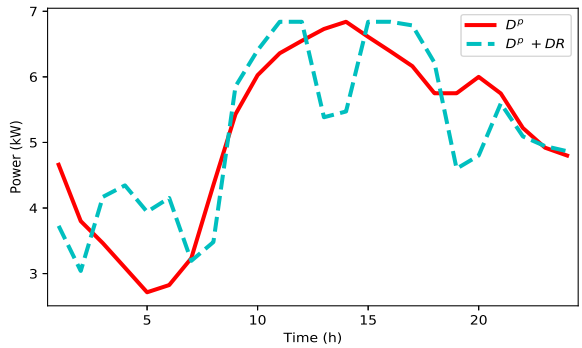

Fig. 7. Active demand with DR.

SOCP-EMS model provides a global optimal solution with reduced computation cost. Hence, it can be used in optimizing islanded MG scheduling.

The islanded MG scheduling for each case study is provided in the following.

1) Case I: In this case, all the generation and storage units are online. Fig. 6 shows the scheduled power profiles of DG, PV, TT, and battery. DG will remain ON all the time, as RESs and battery cannot meet the load demand. The battery is charging during high TT and PV output power. It discharges to provide supply to load ends when PV system and TT have low or no output power. The active power demands before and after DR are shown in Fig. 7. After DR, the load increases to use excess TT output power during $t = 3$ h to $t = 6$ h, as the demand is minimum during this period. The load decreases at $t = 7$ h and $t = 8$ h because of low availability of PV's output power. Then load increases again during high power outputs of both TT and PV system, and it decreases at the peak demand period.

The DR profile at each load bus is presented in Fig. 8. Bus 2 recovers shifted RL at high generation power periods of both PV

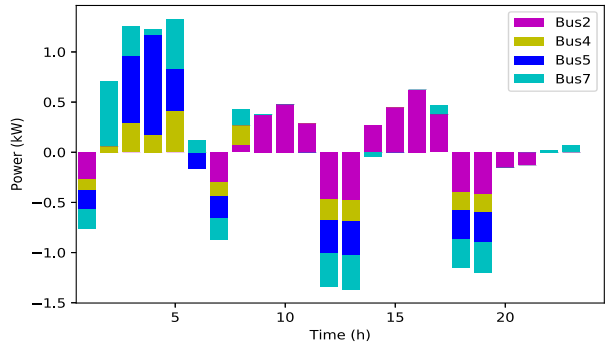

Fig. 8. DR profile at load buses.

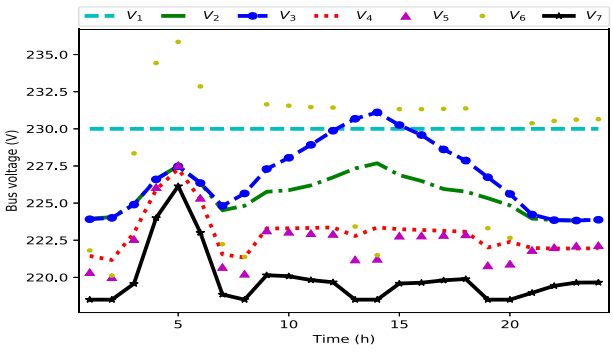

Fig. 9. Buses voltage profile.

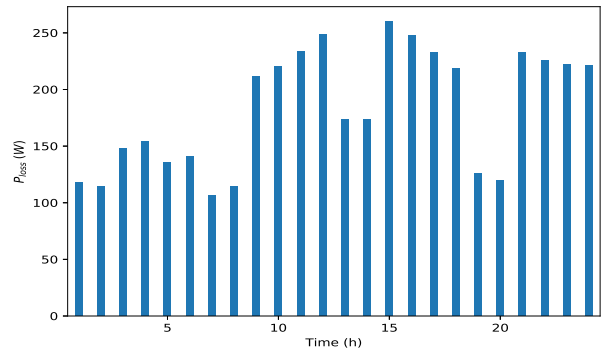

Fig. 10. Active power losses of the islanded MG system.

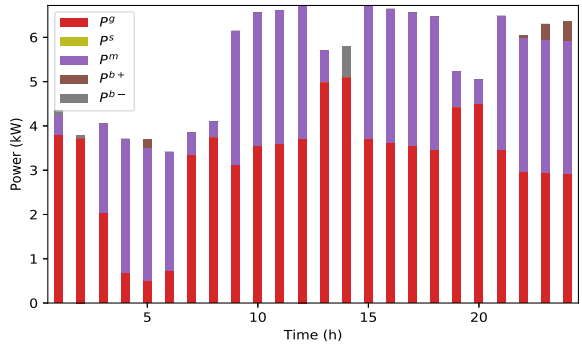

Fig. 11. Islanded MG scheduling profile with no PV power output.

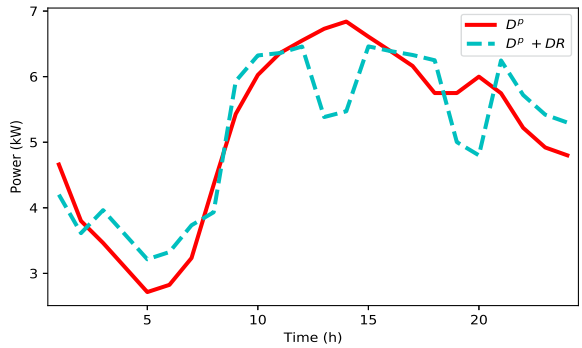

Fig. 12. Active demand with DR, with no PV power output.

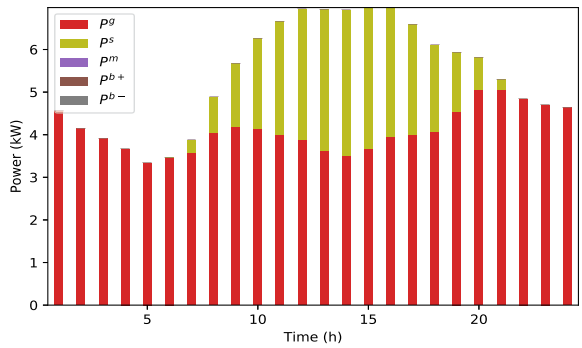

Fig. 13. Islanded MG scheduling profile with no tidal power output.

system and TT, which is shifted from low generation periods. While, buses 4, 5, and 7 shift RL from high demand and low TT output power periods to low demand period. Fig. 9 shows the voltage profiles of the islanded MG network buses. Bus 1, DG bus, is taken as a root bus; therefore, its voltage will remain the same at 230 V. The variations in buses' voltages remain within the specified operational limits of $\pm$ 5%. The active losses of the islanded MG network are shown in Fig. 10. They vary with the load demand. They are higher at high demand periods, but they do not go beyond the specified losses threshold.

2) Case II: In this case, the PV system is considered off-line. The power scheduling profiles of DG, TT, and battery are presented in Fig. 11. The TT and battery cannot meet the load demand. Therefore, DG remains ON all the time. The battery is discharging at $t = 2$ h to $t = 14$ h when TT does not produce power. The battery is charging during low demand and high TT power periods. Fig. 12 shows the active-power demand profile with and without DR. It clearly shows that DR has shifted RL from low to high TT power output periods to avoid DG to produce more power.

3) Case III: In this case, TT is assumed off-line. Fig. 13 shows that the TT is off-line and that it is producing no power. Only DG and PV system produce power to meet load demand. The PV system does not produce excess power to meet all load demand and charge battery. Hence, the battery will not charge or discharge during the 24-h scheduling period. Fig. 14 shows that the DR shifts RL from peak demand to low demand periods to

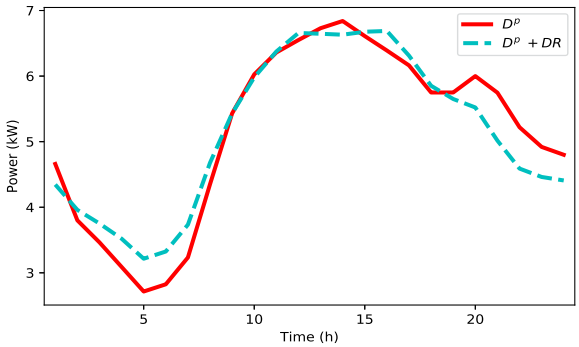

Fig. 14. Active demand with DR, with no tidal power output.

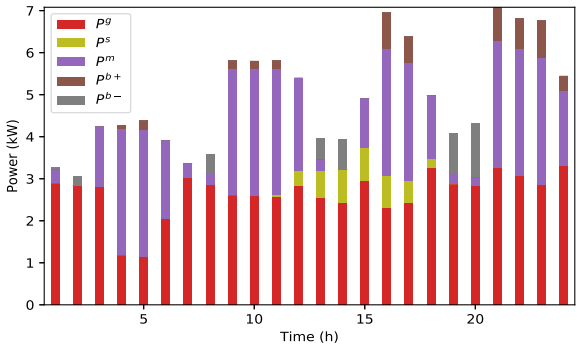

Fig. 15. Islanded MG scheduling profile in December.

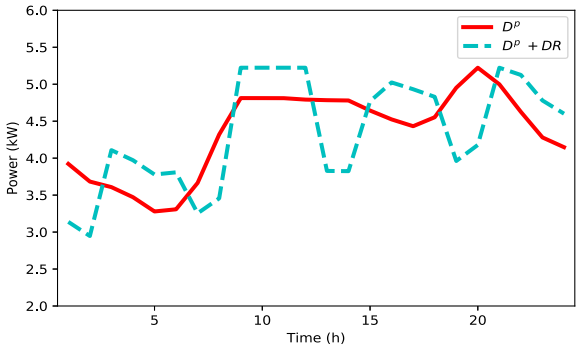

Fig. 16. Active demand with DR in December.

reduce network losses. Moreover, DG will produce lesser power at peak periods.

4) Case IV: In this case, the islanded MG scheduling is studied for 24-h period in December. The PV system produces lesser power in December at Ouessant island, as shown in Fig. 15. It clearly shows that the PV system could only produce small amount of power from $t = 11$ h to $t = 18$ h. The battery charges at high TT power production periods and discharges when TT and PV system produce less or no power. Fig. 16 shows the active-power demand profile with and without DR. The DR load shifts from peak demand periods. The shifted DR load is recovered at low demand and high TT power output periods. This DR shift reduces network losses and decreases the use of DG power production at peak demand periods.

TABLE IV
ISLANDED MG EMISSIONS

	Case A	Case B	Case C	Case D
Emissions (kg)	99.45	76.68	60.89	37.35

B. Emissions Reduction

In this section, we investigate the reduction in the emissions of the islanded MG. It contains DG unit, which produces high GHG emissions against each one kWh unit of electric power production. RESs can be integrated in an islanded MG to reduce DG emission. Therefore, the following four cases have been considered to study the effects of RESs integration in decreasing the islanded MG emissions:

1) Case A: DG only;
2) Case B: DG, PV, and battery;
3) Case C: DG, TT, and battery;
4) Case D: DG, PV, TT, and battery.

In Case A, DGs have been installed at Buses 1, 3, and 6, respectively. All the DGs' specifications are similar. In Case B, DG, PV system, and battery are installed at Buses 1, 3, and 4, respectively. In Case C, DG, battery, and TT are installed at Buses 1, 4, and 6, respectively. While DG, PV system, battery, and TT are installed at Buses 1, 3, 4, and, 6, respectively, for Case D.

Table IV presents the emissions for each case for the 24-h period in July. In Case A, the islanded MG emissions are 99.45 kg. However, they are reduced to 76.68 kg in Case B. In Cases C and D, the emissions are further reduced to 60.89 and 37.35 kg, respectively. The ratio of emissions reduction is 22.9% in Case B. While, it is 38.7 % and 62.4 % in Cases C and D, respectively. Hence, these case studies clearly prove that RESs and battery can be assumed to play a vital role in reducing the emissions in an islanded MG network's operation.

VI. CONCLUSION

In this paper, a convex EMS has been developed for an islanded MG that optimizes its operating and emission costs. DG operating and emission costs are modeled. Levelized cost of energy models were developed for TT and PV system. Battery degradation cost was also formulated, which includes temperature- and DOD-dependent aging effects. An incentive-based DR and MG network model were also incorporated in the EMS to facilitate the active participation of consumers and to satisfy system constraints. The developed second-order cone programming model has achieved the global optimal solution with a less optimality gap and reduced computational cost. The simulation results have clearly proved the effectiveness of the proposed model, which would aid in the optimal scheduling of islanded MGs in the future.

REFERENCES

[1] M. F. Zia, E. Elbouchikhi, and M. Benbouzid, "Microgrids energy management systems: A critical review on methods, solutions, and prospects," *Appl. Energy*, vol. 222, pp. 1033–1055, 2018.
[2] N. Hatziargyriou, Ed., *Microgrids*. Hoboken, NJ, USA: Wiley, 2013.

[3] N. L. Diaz, A. C. Luna, J. C. Vasquez, and J. M. Guerrero, "Centralized control architecture for coordination of distributed renewable generation and energy storage in islanded AC microgrids," *IEEE Trans. Power Electron.*, vol. 32, no. 7, pp. 5202–5213, Jul. 2017.

[4] J. G. de Matos, F. S. F. e Silva, and L. A. de S. Ribeiro, "Power control in ac isolated microgrids with renewable energy sources and energy storage systems," *IEEE Trans. Ind. Electron.*, vol. 62, no. 6, pp. 3490–3498, Jun. 2015.

[5] J. Huckerby, H. Jeffrey, A. de Andres, and L. Finlay, "An international vision for ocean energy, version–III," Ocean Energy Systems, Lisbon, Portugal, 2017.

[6] H. Boye, E. Caquot, P. Clement, L. de La Cochetiere, J. Nataf, and P. Sergent, "Rapport de la mission d'étude sur les énergies marines renouvelables," Ministère de l'écologie, du développement durable et de l'énergie, Paris, Tech. Rep. N° 2013 / 008693-01 / CGEDD, 2013.

[7] D. Magagna and A. Uihlein, "Ocean energy development in Europe: Current status and future perspectives," *Int. J. Mar. Energy*, vol. 11, pp. 84–104, 2015.

[8] D. Greaves and G. Iglesias, Eds., *Wave and Tidal Energy*. Hoboken, NJ, USA: Wiley, 2018.

[9] A. K. Sleiti, "Tidal power technology review with potential applications in gulf stream," *Renewable Sustain. Energy Rev.*, vol. 69, pp. 435–441, 2017.

[10] O. H. Mohammed, Y. Amirat, M. Benbouzid, S. Haddad, and G. Feld, "Optimal sizing and energy management of hybrid wind/tidal/PV power generation system for remote areas: Application to the Ouessant French island," in *Proc. IECON 42nd Annu. Conf. IEEE Ind. Electron. Soc.*, 2016, pp. 4205–4210.

[11] T. El Tawil, J. F. Charpentier, and M. Benbouzid, "Sizing and rough optimization of a hybrid renewable-based farm in a stand-alone marine context," *Renewable Energy*, vol. 115, pp. 1134–1143, 2018.

[12] M. F. Zia, E. Elbouchikhi, and M. Benbouzid, "An energy management system for hybrid energy sources-based stand-alone marine microgrid," in *Proc. Int. Conf. Smart Power Internet Energy Syst.*, Apr. 2019, pp. 1–8.

[13] L. Meng, E. R. Sanseverino, A. Luna, T. Dragicevic, J. C. Vasquez, and J. M. Guerrero, "Microgrid supervisory controllers and energy management systems: A literature review," *Renewable Sustain. Energy Rev.*, vol. 60, pp. 1263–1273, 2016.

[14] F. Cingoz, A. Elrayyah, and Y. Sozer, "Optimized resource management for PV–fuel-cell-based microgrids using load characterizations," *IEEE Trans. Ind. Appl.*, vol. 52, no. 2, pp. 1723–1735, Mar.–Apr. 2016.

[15] N. Faridnia, D. Habibi, S. Lachowicz, and A. Kavousifard, "Optimal scheduling in a microgrid with a tidal generation," *Energy*, vol. 171, pp. 435–443, 2019.

[16] S. Sukumar, H. Mokhlis, S. Mekhilef, K. Naidu, and M. Karimi, "Mix-mode energy management strategy and battery sizing for economic operation of grid-tied microgrid," *Energy*, vol. 118, pp. 1322–1333, 2017.

[17] A. C. Luna, N. L. Diaz, M. Graells, J. C. Vasquez, and J. M. Guerrero, "Mixed-integer-linear-programming-based energy management system for hybrid PV-wind-battery microgrids: Modeling, design, and experimental verification," *IEEE Trans. Power Electron.*, vol. 32, no. 4, pp. 2769–2783, Apr. 2017.

[18] N. Anglani, G. Oriti, and M. Colombini, "Optimized energy management system to reduce fuel consumption in remote military microgrids," *IEEE Trans. Ind. Appl.*, vol. 53, no. 6, pp. 5777–5785, Nov. 2017.

[19] F. Conte, F. D'Agostino, P. Pongiglione, M. Saviozzi, and F. Silvestro, "Mixed-integer algorithm for optimal dispatch of integrated PV-storage systems," *IEEE Trans. Ind. Appl.*, vol. 55, no. 1, pp. 238–247, Jan.–Feb. 2019.

[20] P. P. Vergara, J. C. López, L. C. da Silva, and M. J. Rider, "Security-constrained optimal energy management system for three-phase residential microgrids," *Elect. Power Syst. Res.*, vol. 146, pp. 371–382, 2017.

[21] B. V. Solanki, K. Bhattacharya, and C. A. Canizares, "A sustainable energy management system for isolated microgrids," *IEEE Trans. Sustain. Energy*, vol. 8, no. 4, pp. 1507–1517, Oct. 2017.

[22] B. V. Solanki, A. Raghurajan, K. Bhattacharya, and C. A. Canizares, "Including smart loads for optimal demand response in integrated energy management systems for isolated microgrids," *IEEE Trans. Smart Grid*, vol. 8, no. 4, pp. 1739–1748, Jul. 2017.

[23] J. S. Giraldo, J. A. Castrillon, and C. A. Castro, "Energy management of isolated microgrids using mixed-integer second-order cone programming," in *Proc. IEEE Power Energy Soc. Gen. Meeting*, 2017, pp. 1–5.

[24] I. Serna-Suárez, G. Ordóñez-Plata, and G. Carrillo-Caicedo, "Microgrid's energy management systems: A survey," in *Proc. 12th IEEE Int. Conf. Eur. Energy Market*, 2015, pp. 1–6.

[25] T. El Tawil, N. Guillou, J. F. Charpentier, and M. Benbouzid, "On tidal current velocity vector time series prediction: A comparative study for a French high tidal energy potential site," *J. Mar. Sci. Eng.*, vol. 7, no. 2, 46, pp. 1–13, 2019.

[26] N. Guillou, S. P. Neill, and P. E. Robins, "Characterising the tidal stream power resource around France using a high-resolution harmonic database," *Renewable Energy*, vol. 123, pp. 706–718, 2018.

[27] N. Guillou, G. Chapalain, and S. P. Neill, "The influence of waves on the tidal kinetic energy resource at a tidal stream energy site," *Appl. Energy*, vol. 180, pp. 402–415, 2016.

[28] E. Segura, R. Morales, J. Somolinos, and A. López, "Techno-economic challenges of tidal energy conversion systems: Current status and trends," *Renewable Sustain. Energy Rev.*, vol. 77, pp. 536–550, 2017.

[29] Z. Zhou, M. Benbouzid, J.-F. Charpentier, F. Scuiller, and T. Tang, "Developments in large marine current turbine technologies —A review," *Renewable Sustain. Energy Rev.*, vol. 71, pp. 852–858, 2017.

[30] K. Touimi, M. Benbouzid, and P. Tavner, "Tidal stream turbines: With or without a gearbox?" *Ocean Eng.*, vol. 170, pp. 74–88, 2018.

[31] D. Greaves and G. Iglesias, Eds., *Wave and Tidal Energy*. Hoboken, NJ, USA: Wiley, 2018.

[32] M. F. Zia, E. Elbouchikhi, and M. Benbouzid, "Optimal operational planning of scalable DC microgrid with demand response, islanding, and battery degradation cost considerations," *Appl. Energy*, vol. 237, pp. 695–707, 2019.

[33] S. Kundu, S. Backhaus, and I. A. Hiskens, "Distributed control of reactive power from photovoltaic inverters," in *Proc. IEEE Int. Symp. Circuits Syst.*, 2013, pp. 249–252.

[34] V. Calderaro, G. Conio, V. Galdi, G. Massa, and A. Piccolo, "Optimal decentralized voltage control for distribution systems with inverter-based distributed generators," *IEEE Trans. Power Syst.*, vol. 29, no. 1, pp. 230–241, Jan. 2014.

[35] Q. Nguyen, H. V. Padullaparti, K.-W. Lao, S. Santoso, X. Ke, and N. Samaan, "Exact optimal power dispatch in unbalanced distribution systems with high PV penetration," *IEEE Trans. Power Syst.*, vol. 34, no. 1, pp. 718–728, Jan. 2019.

[36] J. A. Taylor, *Convex Optimization Power Systems*. Cambridge, U.K.: Cambridge Univ. Press, 2015.

[37] S. Boyd and L. Vandenberghe, *Convex Optimization*. Cambridge, U.K.: Cambridge Univ. Press, 2004.

[38] S. H. Low, "Convex relaxation of optimal power flow—Part I: Formulations and equivalence," *IEEE Trans. Control Netw. Syst.*, vol. 1, no. 1, pp. 15–27, Mar. 2014.

[39] S. H. Low, "Convex relaxation of optimal power flow—Part II: Exactness," *IEEE Trans. Control Netw. Syst.*, vol. 1, no. 2, pp. 177–189, Jun. 2014.

[40] C. Coffrin, H. L. Hijazi, and P. van Hentenryck, "The QC relaxation: A theoretical and computational study on optimal power flow," *IEEE Trans. Power Syst.*, vol. 31, no. 4, pp. 3008–3018, Jul. 2016.

[41] B. Kocuk, S. S. Dey, and X. A. Sun, "Strong SOCP relaxations for the optimal power flow problem," *Oper. Res.*, vol. 64, no. 6, pp. 1177–1196, 2016.

[42] R. A. Jabr, "Radial distribution load flow using conic programming," *IEEE Trans. Power Syst.*, vol. 21, no. 3, pp. 1458–1459, Aug. 2006.

[43] S. Sojoudi and J. Lavaei, "Physics of power networks makes hard optimization problems easy to solve," in *Proc. IEEE Power Energy Soc. Gen. Meeting*, 2012, pp. 1–8.

[44] L. Gurobi Optimization, "Gurobi optimizer reference manual," 2018. [Online]. Available: http://www.gurobi.com

[45] A. Wächter and L. T. Biegler, "On the implementation of an interior-point filter line-search algorithm for large-scale nonlinear programming," *Math. Program.*, vol. 106, no. 1, pp. 25–57, 2005.

[46] L. Beal, D. Hill, R. Martin, and J. Hedengren, "Gekko optimization suite," *Processes*, vol. 6, no. 8, 106, pp. 1–26, 2018.

[47] N. Pogaku, M. Prodanovic, and T. C. Green, "Modeling, analysis and testing of autonomous operation of an inverter-based microgrid," *IEEE Trans. Power Electron.*, vol. 22, no. 2, pp. 613–625, Mar. 2007.

[48] C. Li, S. K. Chaudhary, M. Savaghebi, J. C. Vasquez, and J. M. Guerrero, "Power flow analysis for low-voltage AC and DC microgrids considering droop control and virtual impedance," *IEEE Trans. Smart Grid*, vol. 8, no. 6, pp. 2754–2764, Nov. 2017.

Muhammad Fahad Zia (S'18) received the B.S. degree in electrical engineering with honors from the University of Engineering and Technology, Lahore, Pakistan, in 2009, and the M.S. degree in electrical engineering from the King Fahd University of Petroleum and Minerals, Dhahran, Saudi Arabia, in 2014. Currently, he is working toward the Ph.D. degree in electrical engineering at the University of Brest, Brest, France.

He was an Assistant Manager (Operations) with the PTCL, Lahore, Pakistan from 2009 to 2010. From 2010 to 2012, he was a Lab Engineer and from 2014 to 2017 a Lecturer and Assistant Professor with the University of Management and Technology, Lahore, Pakistan. His main research interests and experience include ac/dc microgrids, marine microgrids, energy management systems, power electronics, distributed generation and storage, and transactive energy and its applications in microgrids.

Elhoussin Elbouchikhi (S'12–M'18–SM'19) received the Diploma Engineer degree (Dipl.-Ing.) in automatic and electrical engineering and the Research Master's degree in automatic systems, computer science and decision, from the National Polytechnic Institute of Toulouse (INP-ENSEEIHT), Toulouse, France, in 2010, and the Ph.D. degree in electrical engineering from the University of Brest, Brest, France, in 2013.

After receiving the Ph.D. degree, he has been a Post-Doctoral Researcher with the ISEN Brest, Brest, France and an Associate Member with the LBMS Laboratory (EA 4325) from October 2013 to September 2014. Since September 2014, he has been an Associate Professor with the ISEN Brest and is a member with the Institut de Recherche Dupuy de Lôme—IRDL (UMR CNRS 6027). His main current research interests and experience include electrical machines control and faults detection and diagnosis, fault tolerant control in marine current turbines, and signal processing and statistics for power systems monitoring. He is also interested in energy management systems in microgrids and renewable energy applications such as marine currents turbines, wind turbines, and hybrid generation systems.

Mohamed Benbouzid (S'92–M'94–SM'98) received the B.Sc. degree in electrical engineering from the University of Batna, Batna, Algeria, in 1990, the M.Sc. and Ph.D. degrees in electrical and computer engineering from the National Polytechnic Institute of Grenoble, Grenoble, France, in 1991 and 1994, respectively, and the Habilitation à Diriger des Recherches degree from the University of Picardie "Jules Verne," Amiens, France, in 2000.

After receiving the Ph.D. degree, he joined the Professional Institute of Amiens, University of Picardie "Jules Verne," where he was an Associate Professor of electrical and computer engineering. Since September 2004, he has been with the University of Brest, Brest, France, where he is a Full Professor of electrical engineering. He is also a Distinguished Professor and a 1000 Talent Expert at the Shanghai Maritime University, Shanghai, China. His main research interests and experience include analysis, design, and control of electric machines, variable-speed drives for traction, propulsion, and renewable energy applications, and fault diagnosis of electric machines.

Prof. Benbouzid is a Fellow of the IET. He is the Editor-in-Chief for the *International Journal on Energy Conversion*. He is also an Associate Editor for the IEEE TRANSACTIONS ON ENERGY CONVERSION and the IEEE TRANSACTIONS ON VEHICULAR TECHNOLOGY. He is a Subject Editor for the *IET Renewable Power Generation*.

Josep M. Guerrero (S'01–M'04–SM'08–F'15) received the B.S. degree in telecommunications engineering, the M.S. degree in electronics engineering, and the Ph.D. degree in power electronics, from the Technical University of Catalonia, Barcelona, Spain, in 1997, 2000, and 2003, respectively.

Since 2011 he has been a Full Professor with the Department of Energy Technology, Aalborg University, Aalborg, Denmark, where he is responsible for the Microgrid Research Program (www.microgrids.et.aau.dk). He has been a Chair Professor with the Shandong University since 2014, a Distinguished Guest Professor with Hunan University, Changsha, China, since 2015, and a Visiting Professor Fellow with Aston University, Birmingham, U.K, and a Guest Professor with the Nanjing University of Posts and Telecommunications, Nanjing, China, since 2016. He became a Villum Investigator in 2019. His research interests are oriented to different microgrid aspects, including power electronics, distributed energy-storage systems, hierarchical and cooperative control, energy management systems, smart metering and the Internet of Things for ac/dc microgrid clusters and islanded minigrids, recently specially focused on maritime microgrids for electrical ships, vessels, ferries and seaports.

Prof. Guerrero is an Associate Editor for a number of IEEE journals. He has authored or coauthored more than 500 journal papers in the fields of microgrids and renewable energy systems, which have been cited more than 30 000 times. He was the recipient of the Best Paper Award of the IEEE TRANSACTIONS ON ENERGY CONVERSION for the period 2014–2015, and the Best Paper Prize of IEEE-PES, in 2015. As well, he was the recipient of the Best Paper Award of the Journal of Power Electronics in 2016. During five consecutive years, from 2014 to 2018, he was awarded by Clarivate Analytics (former Thomson Reuters) as Highly Cited Researcher. In 2015, he was elevated to the position of IEEE Fellow for his contributions on "distributed power systems and microgrids."